HHS Public Access

Author manuscript

Epilepsia. Author manuscript; available in PMC 2022 March 07.

Published in final edited form as:

Epilepsia. 2021 December ; 62(12): 3117–3130. doi:10.1111/epi.17082.

Recurrent febrile seizures alter intrahippocampal temporal coordination but do not cause spatial learning impairments

Michelle L. Kloc[1], **Jennifer M. Daglian**[2], **Gregory L. Holmes**[1], **Tallie Z. Baram**[2,3,4], **Jeremy M. Barry**[1]

[1]Department of Neurological Sciences, Epilepsy Development and Cognition Group, Larner College of Medicine, University of Vermont, Burlington, Vermont, USA

[2]Department of Pediatrics, University California, Irvine, Irvine, California, USA

[3]Department of Anatomy/Neurobiology, University California, Irvine, Irvine, California, USA

[4]Department of Neurology, University California, Irvine, Irvine, California, USA

Abstract

Objective: Febrile seizures (FSs) are the most common form of seizures in children. Single short FSs are benign, but FSs lasting longer than 30 min, termed febrile status epilepticus, may result in neurological sequelae. However, there is little information about an intermediary condition, brief recurrent FSs (RFSs). The goal of this study was to determine the role of RFSs on spatial learning and memory and the properties of spontaneous hippocampal signals.

Methods: A hippocampus-dependent active avoidance task was used to assess spatial learning and memory in adult rats that underwent experimental RFSs (eRFSs) in early life compared with their littermate controls. Following completion of the task, we utilized high-density laminar probes to measure spontaneous hippocampal CA1 circuit activity under urethane anesthesia, which allowed for the simultaneous recording of input regions in CA1 associated with both CA3 and entorhinal cortex.

Results: RFSs did not result in deficits in the active avoidance spatial test, a hippocampus-dependent test of spatial learning and memory. However, in vivo high-density laminar electrode recordings from eRFS rats had significantly altered power and frequency expression of theta and gamma bandwidths as well as signaling efficacy along the CA1 somatodendritic axis. Thus, although eRFS modified CA1 neuronal input/output dynamics, these alterations were not sufficient to impair active avoidance spatial behavior.

Correspondence: Jeremy M. Barry, University of Vermont, Larner College of Medicine, 95 Carrigan Dr., 118 Stafford Hall, Burlington, VT 05405, USA. jeremy.barry@med.uvm.edu.

AUTHOR CONTRIBUTIONS

Literature search: M.L.K., J.M.B., G.L.H., T.Z.B.; figures and data analysis: M.L.K., J.M.B.; study design: M.L.K., J.M.B., G.L.H., T.Z.B.; data collection: M.L.K. All authors wrote the paper.

CONFLICT OF INTEREST

None of the authors has any conflict of interest to disclose. We confirm that we have read the Journal's position on issues involved in ethical publication and affirm that this report is consistent with those guidelines.

SUPPORTING INFORMATION

Additional supporting information may be found in the online version of the article at the publisher's website.

Significance: These findings indicate that although eRFSs do not result in spatial cognitive deficits in the active avoidance task, recurrent seizures do alter the brain and result in longstanding changes in the temporal organization of the hippocampus.

Keywords

coherence; development; febrile seizures; spatial cognition; temporal coordination

1 | INTRODUCTION

Febrile seizures (FSs) in children are associated with a temperature of 38°C or higher and do not occur as a result of an intracranial infection or any metabolic imbalance. FSs are common, affecting 2%–5% of children by 6 years of age,[1] but vary in their severity and outcomes. Most FSs are generalized convulsions that last <10 min, classified as simple FSs. Simple FSs are considered benign, without any long-term effects on cognition in children[2,3] and in animal models.[4] In contrast, FSs presenting with a focal onset or prolonged duration (>10 min), or that occur more than once (recurrently) within the same febrile illness are considered complex. A subclass of complex FSs is febrile status epilepticus (FSE), defined as an FS lasting >30 min. Children with FSE may develop long-term cognitive deficits.[5–8]

In the animal model for early life seizures induced by hyperthermia, experimental FSE (eFSE) in rat pups result in longstanding deficits in spatial cognition in both the Morris water maze and the active avoidance task.[9–12] Cognitive problems that follow eFSE involve aberrant changes in temporal dynamics in the hippocampus.[9–11,13] Whether experimental recurrent FSs (eRFSs), a category of complex FSs, cause cognitive deficits corresponding to a gradient of changes in hippocampal temporal coordination is not well understood.

We reasoned that there may be a continuum of injury following FSs, ranging from none following a simple FS to a mild deficit following eRFSs, and more significant deficits with eFSE. To detect this possible gradient in physiological outcomes, we used high-density electrophysiological probes along the somatodendritic axis of CA1 pyramidal cells in adult rats that had experienced multiple brief FSs during postnatal development.

We found that eRFSs induced during one day of a sensitive period for spatial circuit development (postnatal day [P] 10 or P11)[14] do not result in spatial learning impairments in the active avoidance task. Despite this, following high-density electrophysiological interrogation of CA1 signaling, we report significant changes to the somatodendritic circuit throughput.

2 | MATERIALS AND METHODS

2.1 | Animals and experimental overview

All procedures were approved by the University of Vermont and University of California, Irvine animal care and use committees and conducted in accordance with guidelines from the National Institutes of Health. Behavioral and electrophysiological experiments were conducted on 12 adult male Sprague Dawley rats (control [CTL], $n = 6$; eRFS, $n = 6$) that were individually housed on a regular 12-h light/dark cycle with food and water ad libitum.

Prior to weaning, brief repetitive FSs were induced in rat pups at age P10 or P11. Once rats were >P50, they underwent a behavioral assessment of spatial cognition, followed by a terminal acute electrophysiological assessment under anesthesia (P60–P80). Data from our laboratory[15] has shown that female rats do not exhibit cognition deficits following early life seizures; therefore, male rats were used in this study to prioritize the correlation of physiological changes with (possibly) impaired cognition.

2.2 | FS induction

Repeated FSs were induced at P10–P11 as previously described.[11–13] Warm air was continuously infused over the rat pups until hyperkinesis and seizure behaviors (freezing, chewing) were observed. To maintain core body temperature above 39°C, warm air was infused for 20–60 s every 2 min for a total time of 60 min. Pup temperature was measured every 2 min, after heating, and maintained between 38.5°C and 41°C. The presence or absence of FSs was observed continuously, and seizures were scored for their duration and phenotype. Electroencephalograms (EEGs) were not recorded during FS induction, necessitating a behavioral measure of seizure severity to compare seizures across animals and litters. Rat behavior during FSs is consistent with the Racine scale; therefore, Racine stages were used to characterize seizure intensity. This included stages of (1) mouth and facial movement, (2) head nodding (3) forelimb clonus, (4) rearing with forelimb clonus, and (5) rearing and falling with forelimb clonus. The protocol employed here led to repeated seizures over the course of 60 min (5–8 seizures per rat) to simulate multiple FSs within a single illness. Notably, the seizures were brief and repetitive. Average total time spent in seizure was 11 ± 2.3 min (Table S1). To control for maternal deprivation stress, which can exacerbate cognitive deficits following early life seizures,[16] weight-matched normothermic littermates were separated from their dams for the duration of the eRFS induction period and maintained in a separate container on a warming pad (~1 h). At the end of the procedure, eRFS pups and their weight-matched maternally deprived control littermates were returned to their home cage and dam.

2.3 | Active avoidance

The active avoidance task is a hippocampal-dependent task that requires functional connectivity between multiple brain regions.[17–21] To measure spatial learning and memory, a hippocampus-dependent active avoidance task was used as described previously.[10,11,13] Adult rats (aged 2 months) were anesthetized with isoflurane and implanted with a stainless-steel clip (Eagle Claw) in the skin of their upper back, between the forelimbs, 18–24 h prior to the task. Rats were placed on a constantly rotating arena (diameter = 82 cm) containing an unmarked zone occupying a 60° arc that corresponds with the delivery of an aversive shock (.4 mA). A cable with light-emitting diode was attached to the clip to deliver the shock when a zone entry was detected. Rats must learn to continuously avoid the unmarked shock zone (Figure 1A,B) using unique visual cues in the room, located distally outside of the arena. A rat reaches learning criterion when it receives five or fewer shocks in two consecutive sessions. Rats were habituated to the arena for 10 min at the start of the experiment, and then completed sixteen 10-min trials across 2 days (eight trials per day). Behavioral data, including number of shocks and time spent in each zone of the arena, were analyzed using TRACK ANALYSIS software (Bio-Signal Group).

2.4 | Surgery and electrophysiological recording

Following assessment of spatial cognition on the active avoidance task, wideband local field potentials (LFPs; 1–6000 Hz, sampling rate = 30.3 kHz) were recorded across the depth of the CA1 from adult rats. One CTL rat died following anesthesia induction before recordings could be obtained (LFP recordings: CTL, $n = 5$; eRFS, $n = 6$). LFPs were measured using a 64-channel laminar silicon probe (interelectrode distance = 20 μm; H3, Cambridge NeuroTech). Rats were anesthetized with urethane (1.6–1.7 mg/kg in sterile saline; Sigma Aldrich) injected intraperitoneally. Subjects were affixed in a stereotaxic frame, and the surface of the skull was cleared of tissue. Dorsal hippocampus was located bilaterally at −4 mm anteroposterior/2.2–2.5 mm mediolateral relative to bregma. A large burr hole craniotomy was drilled (2.3 mm), and the dura was removed. The probe, attached to a digital multiplexing headstage, was slowly lowered in 1-mm intervals at ~.05 mm/s every 10–15 min until the tip of the probe was located in the hilar region of the dentate gyrus. Probe position was secondarily determined relative to CA1 stratum pyramidale (SP; probe channels 7–11; probe depth = 120–200 μm; Figure 2). All depth results are relative to probe channel 1 in stratum oriens (SO). Experiment-to-experiment position variability was generally limited to 20–80 μm. At maximum depth, continuously sampled LFP recordings were made via the DigitalLynx SX acquisition system and Cheetah software (v6.4, Neuralynx) for a minimum of 1 h to ensure that cell firing activity and EEG quality were stable.

2.5 | Electrophysiological data analysis

2.5.1 | Spectral properties—Power and frequency band properties were analyzed for theta (4–12 Hz), slow gamma (30–50 Hz), and medium gamma (70–90 Hz) bandwidths to address physiological changes in temporal organization, synaptic inputs from CA3, and neocortical synaptic inputs, respectively, using custom MATLAB scripts as described previously,[22] using the MATLAB signal processing toolbox “spectrogram” function (MATLAB v2019a; MathWorks).

2.5.2 | Coherence and voltage correlation—Coherent oscillatory activity was calculated as a measure of signal phase coordination along the somatodendritic axis[23,24] referenced to the distal-most input region of CA1 apical dendrites at stratum lacunosum moleculare (SLM). The magnitude-squared coherence estimate was applied to determine coherence across groups as a function of depth and frequency. The magnitude-squared coherence is a function of the power spectral densities, $P_{xx}(f)$ and $P_{yy}(f)$, and the cross power spectral density, $P_{xy}(f)$, of x and y. To further evaluate CA1 signal coordination on the somatodendritic axis, amplitude cross-correlation in both groups was analyzed as a function of depth using custom code.[25] LFPs were bandpass filtered, and instantaneous amplitude was calculated. The amplitudes between the target and reference EEG were cross-correlated, and the time lag at which the cross-correlation peak occurs was determined. The distribution of lag times was tested to determine whether they differed from zero. The analysis returned a lag vector containing time lags between peak amplitudes across the analysis window −100 ms to +100 ms and the cross-correlation of the bandpass-filtered amplitudes for the target and reference EEG.

2.5.3 | Single unit analysis—Unit activity was filtered from LFP recordings and clustered using the automated spike-sorting software Kilosort2 extension for MATLAB.[26] All units were examined using the Python-based visualization software Phy[27] and manually reviewed and combined or cleaned as needed. Extracellular action potentials from CA1 SP were only included in subsequent analysis if they exhibited (1) an average unit amplitude > 50 μV, (2) a total spike count of >200 spikes and a firing rate of <9 Hz, and (3) a waveform shape consistent with excitatory neurons,[28,29] and (4) an autocorrelogram shape representing a refractory period of >1 ms that did not display characteristics of multiunit activity. Mean unit amplitude, firing rate, and spike times were taken directly from Kilosort.

Phase preference for each cell relative to each bandwidth of interest was analyzed as previously described.[11,22] As urethane decreases spontaneously expressed theta oscillation frequency in comparison with awake behaving rats,[30] a 2–10-Hz range was specified as theta range. LFPs were filtered using a Chebyshev type 2 filter and phase was extracted using a Hilbert transform; spike times were extracted from Kilosort. The trough of the oscillation cycle was denoted as 0°/360°, and the peak of each cycle was denoted as 180°. The phase angle and mean resultant length (RBAR) of the phase vector for each cell in the CTL and eRFS groups were calculated and plotted for each target region of CA1 (SP, stratum radiatum [SR], SLM) and for two different LFP frequency bandwidths. The circular mean of each cell in each group was determined by averaging the angle value of each spike and dividing by the total spike count. RBAR was calculated using Equation 1:

$$\mathrm{RBAR} = n \times r \tag{1}$$

Where n is the sum of the number of incidences in cases of binned angle data and r is the resultant vector length of the distribution. Greater RBAR values indicate a higher degree of preference to phase.

2.6 | Statistics

All data described are presented as mean ± SE. For all statistical tests, $p < .05$ was considered significant. For active avoidance behavior, the primary outcome measure is the number of shocks. A generalized linear model (GLM; IBM SPSS v26.0) was used to generate a Wald chi-squared statistic to determine whether there were any significant differences within and between groups.

For LFP data, including spectral properties, coherence, voltage correlation, phase lag, and waveform symmetry, GLM analysis was used to determine significant interactions of group, frequency, and depth as noted in the Results. GLM was used to test for main group effect and main depth effect, and channel by channel between groups by depth to provide a detailed understanding of what signals/properties were significantly different as a function of location. The model was adjusted according to the distribution of each analyzed variable, that is, tweedie probability distributions (including the purely continuous normal, gamma, and inverse Gaussian distributions) with log link models were used for nonparametrically distributed data, whereas Poisson log linear distributions were used for count data. Goodness of fit was determined using the corrected quasilikelihood under independence model criterion.

For cell firing data, sample size denotes individual neurons. Statistical differences between mean unit amplitudes across groups were determined using a Mann–Whitney test, a nonparametric test for two unpaired groups of data that is primarily sensitive to changes in the mean. The nonparametric Kolmogorov–Smirnov test was used to compare the cumulative distributions of the two datasets (Prism, GraphPad Software). For phase preference analysis, circular statistics for phase preference were evaluated using the Rayleigh test for nonuniformity of nonlinear data[31] using the Circular Statistics Toolbox in MATLAB.[32]

The experimenter was blind to treatment group throughout all experiments and most data analysis. The blind was broken after active avoidance analysis and most electrophysiological analysis (spectral properties, coherence, voltage correlation, phase lag, waveform symmetry) was complete. The experimenter was aware of group treatment throughout single unit analysis but analyzed the data randomly and organized the data into appropriate groups after the analysis was complete. For all analyses of electrophysiological properties (spectral properties, coherence, etc.), data were plotted individually for each rat to assess whether the rats that could not learn the task were outliers physiologically (data not shown). Learner/nonlearner status did not correlate with aberrant patterns of physiological activity; therefore, all rats were included in the electrophysiological analysis regardless of their ability to learn the task.

3 | RESULTS

3.1 | eRFSs do not impair spatial memory in the absence of status epilepticus

In both CTL ($n = 6$) and eRFS ($n = 6$) groups, one rat did not reach learning criterion (Figure 1C,D). GLM referenced against CTL Session (S) 16 showed no statistically significant differences within or across groups for the number of shocks received (CTL: S1 Wald = .14, $p = .71$; eRFS: S1 Wald = .56, $p = .45$; eRFS: S16 Wald = .24, $p = .63$). Time spent in each zone (Figure 1E) can be a measure of spatial learning strategy[11,13]; if a rat spends the majority of its time in the zone opposite the shock zone, the rat is continuously relocating its position relative to the distal cues in the room and uses an allothetic spatial strategy. Time in zone did not significantly differ between the CTL and eRFS groups with (GLM main group effect, Wald = .95, $p = .76$) or without (GLM main group effect, Wald = 0, $p = .998$) the animal in each group that did not reach task criterion (see Supplementary Results). Both groups therefore used a spatial, rather than a nonspatial, avoidance strategy. Taken together, these results confirm that repeated FSs in early life did not impair spatial learning and memory as measured by the active avoidance task.

3.2 | eRFSs alter spectral properties throughout CA1

High-density LFP recordings in both CTL and eRFS rats allowed for the detailed study of CA1 circuit throughput (Figure 2). From SR to SLM of both groups, peak and normalized theta power and frequency were highest in SLM and lowest in SP (Figure 3A–C; Table S2 rows 1–3). Peak theta power was not statistically different across groups or hippocampal depth measures (Figure 3A; Table S2 row 4), suggesting that the maximal extent of spontaneous synaptic activity under urethane anesthesia was unchanged by eRFSs. When

normalized to the peak, eRFS theta power was significantly lower in SP, superficial SR, and SLM (Figure 3B; Table S3 rows 1–2). Across the somatodendritic axis, eRFS theta frequency was also significantly lower than in CTL (Figure 3C; Table S3 row 3).

eRFS slow gamma oscillations were altered versus CTL. In both groups, the trough of peak slow gamma power was in SP. eRFS peak SR slow gamma was significantly lower than in CTL (Table S3 row 4), yet normalized slow gamma power was similar in both groups (Figure 3B, Table S2 row 5) and was lowest in SP (Table S2 row 6) and highest in mid-SR to dentate gyrus. As a mirror image of normalized slow gamma power, slow gamma frequency was significantly higher in SP-SO than in SLM (Table S2 row 7) and lowest beyond SR (not significant). Notably, eRFS slow gamma frequency was significantly increased throughout SP, SR, SLM, and dentate molecular region (MOL) versus CTL (Figure 3C; Table S3 row 5).

Peak medium gamma power was highest in SR/SLM in both groups, and lowest in SO (Figure 3A; Table S2 rows 8–9). However, eRFS normalized medium gamma power was significantly higher than CTL in the SP, SLM, and dentate MOL (Table S3 rows 6–8). As with slow gamma, medium gamma frequency was highest in SP and there was no significant difference between eRFS and CTL groups (Table S2 row 10). Compared with SLM, medium gamma frequency was significantly higher in SO, SP, and superficial SR, with little fluctuation elsewhere in CA1 (Figure 3C; Table S3 row 9).

In eRFS animals, theta was smaller and slower, whereas slow gamma was smaller and faster. eRFS normalized medium gamma was also significantly larger than CTL in SLM. Slow gamma oscillations are associated with rhythmic synaptic activation of CA3 inputs via Schaffer collaterals that synapse in the SR region, whereas SLM medium gamma is associated with neocortical synaptic activation (specifically in entorhinal cortex [EC]).[33–35] Changes in gamma signal properties may therefore reflect alterations in hippocampal circuit physiology and throughput, ultimately affecting the balance of theta and gamma on cell timing.

3.3 | eRFSs decrease signal coordination between CA1 layers

Phase coherence and voltage correlation along the CA1 somatodendritic axis were calculated to evaluate the efficacy of intrahippocampal communication in each group for theta, slow gamma, and medium gamma as a function of depth (Figure 4A). Referenced to SLM, GLM analysis tested for significant coherence × depth × group interactions in each bandwidth of interest.

eRFS theta oscillations referenced to SLM were significantly less coherent than CTL in SO, SP, and superficial SR (Table S4 rows 1–2). eRFS slow gamma was significantly less coherent than CTL in SO, superficial SP, and throughout deeper SP, SR, and superficial SLM (Table S4 rows 3–5). eRFS medium gamma was also significantly less coherent than CTL in superficial SP, deep SP, SR, and superficial SLM (Table S4 rows 6–7). To break down changes in phase coherence by specific frequency, probe depths corresponding to SP (100–180 μm) and SR (280–400 μm) were averaged and GLM was used to compare group × frequency interactions. SP coherence GLM analysis showed that eRFS theta, beta

(15–25 Hz), and slow gamma coherence was significantly lower than CTL (Figure 4B; Table S5 rows 1–2). Similarly, SR coherence group × frequency analysis showed that eRFS oscillations were less coherent than CTL across most frequency bandwidths, including theta, slow gamma, and medium gamma (Figure 4C; Table S5 row 3).

The profile of voltage correlations across CA1 for each frequency bandwidth (Figure 4E) follows a similar pattern as phase coherence, suggesting that both power and phase are variably synchronous as a function of depth. Referenced to SLM, eRFS voltage correlations were significantly lower that CTL in the theta, slow gamma, and medium gamma bandwidths at many depths throughout the SR and SLM regions. Decreased correlation in the slow gamma range even extended as far as dentate MOL (see Table S6). The voltage correlation time lag was analyzed as a comparison of the temporal properties of the target and reference EEG used in the voltage correlation analysis. CTL theta has a clear peak and trough, whereas eRFS is static (Figure 4D). Lag time analysis showed a significant interaction between CTL and eRFS in CA1 SR (GLM channel-by-channel depth × group comparison: probe depth = 200 μm [Wald = 5.54, $p = .02$] – 280 μm [Wald = 3.89, $p = .048$]).

In CTL animals, both coherence and voltage correlation follow a distinct pattern as afferent synaptic input signals ascend the somatodendritic axis. The alteration of phase coherence and voltage correlation across bandwidths in eRFS animals reflects altered efficacy with which CA1 neuronal dendrites receive, sum, and relay afferent synaptic inputs from various regions, including CA3 and EC.

3.4 | eRFS CA1 neurons exhibit different properties and phase preference

Wideband recordings of hippocampal oscillations also measured spontaneous action potential firing of CA1 neurons (Figure 5A–D). Only excitatory neurons localized to SP (probe depth = 100–180 μm) were included in the analysis (see Materials and Methods). eRFS mean unit amplitude was significantly higher than CTL (CTL, 74.7 ± 5.6 μV, $n = 19$; eRFS, 121.9 ± 10.6 μV, $n = 20$; $p < .0001$; Mann–Whitney test; Figure 6A). Because single unit amplitude can be dependent on the distance of the neuron from the probe site, we also examined single unit firing rate. Single unit firing rate (Figure 6B) distribution around the mean was significantly higher than CTL (CTL, 2.24 ± .6 spikes/s, $n = 19$; eRFS, 3.12 ± .5 spikes/s, $n = 20$; $p = .0485$; Kolmogorov–Smirnov test), further suggesting eRFS neuron temporal organization is altered.

A representative rose plot is shown in Figure 6C, illustrating the general phase preference of action potentials from a single neuron in CA1 SP. CTL and eRFS neurons showed strongest phase preference for bandpass-filtered LFPs for either low (2–10 Hz, delta–theta) or high (70–90 Hz, medium gamma) frequencies (Figure 5B,D), respectively; therefore, only those will be discussed here in SP, SR, and SLM (CTL, $n = 18$; eRFS, $n = 15$; Figure 6D–G). For slow gamma phase preference, see Figure S2.

Control neurons had significant phase preference to the lower frequency bandwidth (Figure 6D) in SLM (angle = 87.66°, RBAR = .51, $p = .015$), SR (angle = 22.3°, RBAR = .59, $p = .004$), and SP (angle = 354.7°, RBAR = .58, $p = .004$), which showed a consistent RBAR

value and an incremental decrease in phase angle moving from SLM toward the soma in SP.[23] Conversely, eRFS neurons did not have a significant 2–10-Hz phase preference relative to any reference region (SLM, angle = 292.8°, RBAR = .4, $p = .055$; SR, angle = 336.3°, RBAR = .25, $p = .31$; SP, angle = 218.3°, RBAR = .08, $p = .88$; Figure 6D) and RBAR decreased in a linear fashion from SLM to SP. CTL neurons exhibited no medium gamma phase preference in SLM (angle = 227.5, RBAR = .35°, $p = .16$) or SR (angle = 264.13°, RBAR = .24, $p = .41$) regions, but showed significant preference to medium gamma in the SP region (angle = 10.9°, RBAR = .45, $p = .043$; Figure 6E). The eRFS neuron population likewise did not significantly prefer medium gamma in SLM (angle = 209.1°, RBAR = .31, $p = .17$), but showed significant phase preference to medium gamma in SR (angle = 327.7°, RBAR = .63, $p < .001$) and SP (angle = 19.2°, RBAR = .73, $p < .0001$; Figure 6F).

Following eRFSs, CA1 neuronal action potentials are on average faster and exhibit phase preference to faster frequencies, whereas CTL neurons exhibit phase preference to slower frequencies. These findings indicate that eRFS CA1 output is less likely to be organized by theta oscillations and more likely to be organized by fast oscillations.

4 | DISCUSSION

The goal of this study was to determine the impact of eRFSs on temporal dynamics within the hippocampus. In the hyperthermia model for early life eFSE, previous studies have identified structural and functional changes associated with impaired cognition,[9–11,13] but the impacts of eRFSs on cognition and hippocampal signaling have been poorly understood in the animal model. Here, we have shown that early life eRFSs occurring without status epilepticus can significantly alter CA1 neuronal input/output dynamics. Notably, these alterations were not sufficient to impair behavior on a hippocampus-dependent spatial active avoidance task.

One important innovation of this study was the use of high-density laminar probes to interrogate the CA1 circuit, which allowed for the simultaneous recording of input regions in CA1 associated with both CA3 and EC. This incremental record of LFPs across the somatodendritic axis provided a means to describe changes both to synaptic signaling, the efficacy of information transfer from input regions of SLM and SR to SP, and cell firing activity.

The rotating arena active avoidance task is a complex task requiring multiple brain regions, but it may not completely characterize behavioral outcomes of eRFSs and their associated signaling deficits. In the FMR1 knockout model,[36] animals sufficiently learn the active avoidance task, but fail to relearn the task once the aversive shock zone is rotated, suggesting a lack of cognitive flexibility. With additional measures, it is possible that subtle behavioral deficits in the eRFS model corresponding to the changes in CA1 circuit input/output dynamics could be identified.

Slow gamma in SR, as generated by synaptic activity arising from CA3 inputs, has been theorized to be associated with memory recall, whereas medium gamma with synaptic activity arising from EC largely innervating SLM is associated with sensorimotor

integration.[33–35] Previous work in the eFSE model identified altered connectivity and temporal organization of inputs to CA1.[10,11,13] It is of interest that most field potential changes relative to CA1 physiology after eRFS were localized to SR and the bandwidth most predominantly altered was gamma.

Our data describing alterations to slow gamma in eRFSs imply CA3 synapses have altered compositions or are reduced in quantity, although the altered theta wave symmetry in SR revealed with cycle-by-cycle analysis (see Supplementary Results and Figure S1) suggest the former. We did not report a clear effect of slow gamma on cell timing on CTL neurons (Figure S2), suggesting slow gamma may have relatively low influence on the CA1 temporal organization under urethane anesthesia. It is possible that the eRFS-specific increased slow gamma coherence in SP may account for the significant phase preference to slow gamma in that layer (angle = 24.4°, RBAR = .437, $p = .029$), yet these data are difficult to interpret considering the lack of preference in CTL (Figure S2). It is known that urethane decreases the frequency of theta oscillations that are spontaneously expressed compared with awake behaving rats,[30] but this effect has not been mirrored at higher frequency bandwidths. This likely accounts for the CTL phase preference for the 2–10-Hz range.

The early life hyperthermia seizure model was developed as a model for comorbid cognitive impairments of FSE, and is therefore specifically timed to correlate with the age in children who experience FSE.[37] The hippocampus develops during the first three weeks of life, but EC grid cells do not fully develop until ~P21.[38] It is possible that the refinement of synaptic activity arising from EC develops normally as the weanling animal begins to navigate its environment, integrate sensory cues, and remember its position, thus becoming the dominant input during the recovery phase after seizures. There is clearly a disruption of signal propagation as inputs ascend the apical dendrites of CA1 neurons, and the observation that neurons are more effectively tuned to EC after eRFSs rather than hippocampal theta could serve as a compensatory mechanism for spatial memory.

Future studies must examine whether alternative behavioral tasks may uncover a deficit in learning and memory and whether cognitive outcome post-eFSE is determined by exceeding a particular threshold of physiological changes to local microcircuitry, synapses, or dendritic morphology[13] in CA1 pyramidal cells, or by the disruption of additional intra- or extrahippocampal structures such as dentate granule cells and EC, respectively.

Supplementary Material

Refer to Web version on PubMed Central for supplementary material.

ACKNOWLEDGMENTS

This work was supported by National Institutes of Health grants NS108765 (J.M.B. and G.L.H.) and NS108296 (J.M.B., G.L.H., and T.Z.B.). We thank Dr. Joshua Gordon and Dr. Avishek Adhikari for sharing code for voltage correlation analysis.

Funding information

National Institute of Neurological Disorders and Stroke, Grant/Award Number: NS108765 and NS108296

REFERENCES

1. Shinnar S, Glauser TA. Febrile seizures. J Child Neurol. 2002;17(Suppl 1):S44–52. [PubMed: 11918463]
2. Verity CM, Greenwood R, Golding J. Long-term intellectual and behavioral outcomes of children with febrile convulsions. N Engl J Med. 1998;338:1723–8. [PubMed: 9624192]
3. Chang YC, Guo NW, Wang ST, Huang CC, Tsai JJ. Working memory of school-aged children with a history of febrile convulsions: a population study. Neurology. 2001;57(1):37–42. [PubMed: 11445625]
4. Chang YC, Huang AM, Kuo YM, Wang ST, Chang YY, Huang CC. Febrile seizures impair memory and cAMP response-element binding protein activation. Ann Neurol. 2003;54(6):706–18. [PubMed: 14681880]
5. Weiss EF, Masur D, Shinnar S, Hesdorffer DC, Hinton VJ, Bonner M, et al. Cognitive functioning one month and one year following febrile status epilepticus. Epilepsy Behav. 2016;64(Pt A):283–8. [PubMed: 27794237]
6. Hesdorffer DC, Benn EK, Bagiella E, Nordli D, Pellock J, Hinton V, et al. Distribution of febrile seizure duration and associations with development. Ann Neurol. 2011;70(1):93–100. [PubMed: 21437934]
7. Scott RC. Adverse outcomes following convulsive status epilepticus in children: relationship with hippocampal injury. Epilepsia. 2010;51(Suppl 3):178–81. [PubMed: 20618427]
8. Scott RC. Consequences of febrile seizures in childhood. Curr Opin Pediatr. 2014;26(6):662–7. [PubMed: 25304962]
9. Barry JM, Choy M, Dube C, Robbins A, Obenaus A, Lenck-Santini PP, et al. T2 relaxation time post febrile status epilepticus predicts cognitive outcome. Exp Neurol. 2015;269:242–52. [PubMed: 25939697]
10. Barry JM, Mahoney JM, Holmes GL. Coordination of hippocampal theta and gamma oscillations relative to spatial active avoidance reflects cognitive outcome after febrile status epilepticus. Behav Neurosci. 2020;134(6):562–76. [PubMed: 32628031]
11. Barry JM, Sakkaki S, Barriere SJ, Patterson KP, Lenck-Santini PP, Scott RC, et al. Temporal coordination of hippocampal neurons reflects cognitive outcome post-febrile status epilepticus. EBioMedicine. 2016;7:175–90. [PubMed: 27322471]
12. Dubé CM, Zhou JL, Hamamura M, Zhao Q, Ring A, Abrahams J, et al. Cognitive dysfunction after experimental febrile seizures. Exp Neurol. 2009;215(1):167–77. [PubMed: 19000675]
13. Patterson KP, Barry JM, Curran MM, Singh-Taylor A, Brennan G, Rismanchi N, et al. Enduring memory impairments provoked by developmental febrile seizures are mediated by functional and structural effects of neuronal restrictive silencing factor. J Neurosci. 2017;37(14):3799–812. [PubMed: 28275159]
14. Baram TZ, Donato F, Holmes GL. Construction and disruption of spatial memory networks during development. Learn Mem. 2019;26(7):206–18. [PubMed: 31209115]
15. Niedecker RW, Kloc ML, Holmes GL, Barry JM. Effects of early life seizures on coordination of hippocampal-prefrontal networks: influence of sex and dynamic brain states. Epilepsia. 2021;62(7):1701–14. [PubMed: 34002378]
16. Huang LT, Holmes GL, Lai MC, Hung PL, Wang CL, Wang TJ, et al. Maternal deprivation stress exacerbates cognitive deficits in immature rats with recurrent seizures. Epilepsia. 2002;43(10):1141–8. [PubMed: 12366727]
17. Vafaei AA, Jezek K, Bures J, Fenton AA, Rashidy-Pour A. Post-training reversible inactivation of the rat's basolateral amygdala interferes with hippocampus-dependent place avoidance memory in a time-dependent manner. Neurobiol Learn Mem. 2007;88(1):87–93. [PubMed: 17408988]
18. Cimadevilla JM, Fenton AA, Bures J. Functional inactivation of dorsal hippocampus impairs active place avoidance in rats. Neurosci Lett. 2000;285(1):53–6. [PubMed: 10788706]
19. Cimadevilla JM, Wesierska M, Fenton AA, Bures J. Inactivating one hippocampus impairs avoidance of a stable room-defined place during dissociation of arena cues from room cues by rotation of the arena. Proc Natl Acad Sci U S A. 2001;98(6):3531–6. [PubMed: 11248112]

20. Lee H, Dvorak D, Kao HY, Duffy AM, Scharfman HE, Fenton AA. Early cognitive experience prevents adult deficits in a neurodevelopmental schizophrenia model. Neuron. 2012;75(4):714–24. [PubMed: 22920261]
21. Rossier J, Kaminsky Y, Schenk F, Bures J. The place preference task: a new tool for studying the relation between behavior and place cell activity in rats. Behav Neurosci. 2000;114(2):273–84. [PubMed: 10832789]
22. Mouchati PR, Kloc ML, Holmes GL, White SL, Barry JM. Optogenetic "low-theta" pacing of the septohippocampal circuit is sufficient for spatial goal finding and is influenced by behavioral state and cognitive demand. Hippocampus. 2020;30(11):1167–93. [PubMed: 32710688]
23. Buzsaki G, Czopf J, Kondakor I, Kellenyi L. Laminar distribution of hippocampal rhythmic slow activity (RSA) in the behaving rat: current-source density analysis, effects of urethane and atropine. Brain Res. 1986;365(1):125–37. [PubMed: 3947979]
24. Brankack J, Stewart M, Fox SE. Current source density analysis of the hippocampal theta rhythm: associated sustained potentials and candidate synaptic generators. Brain Res. 1993;615(2):310–27. [PubMed: 8364740]
25. Adhikari A, Sigurdsson T, Topiwala MA, Gordon JA. Cross-correlation of instantaneous amplitudes of field potential oscillations: a straightforward method to estimate the directionality and lag between brain areas. J Neurosci Methods. 2010;191(2):191–200. [PubMed: 20600317]
26. Pachitariu MSN, Kadir S, Carandini M & Harris KD Fast and accurate spike sorting of high-channel count probes with Kilosort. Adv Neural Inf Process Syst. 2016;4448–56. 30th Conference on Neural Information Processing Systems, Barcelona, Spain.
27. Rossant C, Kadir SN, Goodman DFM, Schulman J, Hunter MLD, Saleem AB, et al. Spike sorting for large, dense electrode arrays. Nat Neurosci. 2016;19(4):634–41. [PubMed: 26974951]
28. Fox SE, Ranck JB. Electrophysiological characteristics of hippocampal complex-spike cells and theta cells. Exp Brain Res. 1981;41(3):399–410. [PubMed: 7215500]
29. Robbins AA, Fox SE, Holmes GL, Scott RC, Barry JM. Short duration waveforms recorded extracellularly from freely moving rats are representative of axonal activity. Front Neural Circuits. 2013;7:181. [PubMed: 24348338]
30. Buzsaki G. Theta oscillations in the hippocampus. Neuron. 2002;33(3):325–40. [PubMed: 11832222]
31. Fisher N Statistical analysis of circular data. Cambridge, UK: Cambridge University Press; 1995.
32. Berens P CircStat: a MATLAB toolbox for circular statistics. J Stat Softw. 2009;31(10):21.
33. Bragin A, Jandó G, Nádasdy Z, Hetke J, Wise K, Buzsáki G. Gamma (40–100 Hz) oscillation in the hippocampus of the behaving rat. J Neurosci. 1995;15(1 Pt 1):47–60. [PubMed: 7823151]
34. Colgin LL. Do slow and fast gamma rhythms correspond to distinct functional states in the hippocampal network? Brain Res. 2015;1621:309–15. [PubMed: 25591484]
35. Colgin LL, Denninger T, Fyhn M, Hafting T, Bonnevie T, Jensen O, et al. Frequency of gamma oscillations routes flow of information in the hippocampus. Nature. 2009;462(7271):353–7. [PubMed: 19924214]
36. Radwan B, Dvorak D, Fenton AA. Impaired cognitive discrimination and discoordination of coupled theta-gamma oscillations in Fmr1 knockout mice. Neurobiol Dis. 2016;88:125–38. [PubMed: 26792400]
37. Baram TZ, Gerth A, Schultz L. Febrile seizures: an appropriate-aged model suitable for long-term studies. Brain Res Dev Brain Res. 1997;98(2):265–70. [PubMed: 9051269]
38. Wills TJ, Barry C, Cacucci F. The abrupt development of adultlike grid cell firing in the medial entorhinal cortex. Front Neural Circuits. 2012;6:21. [PubMed: 22557949]

Key Points

- RFSs during early life do not cause spatial learning impairments as measured by the active avoidance task
- eRFS-induced changes to somatodendritic circuit throughput suggest an altered balance in the input/output dynamics of CA1

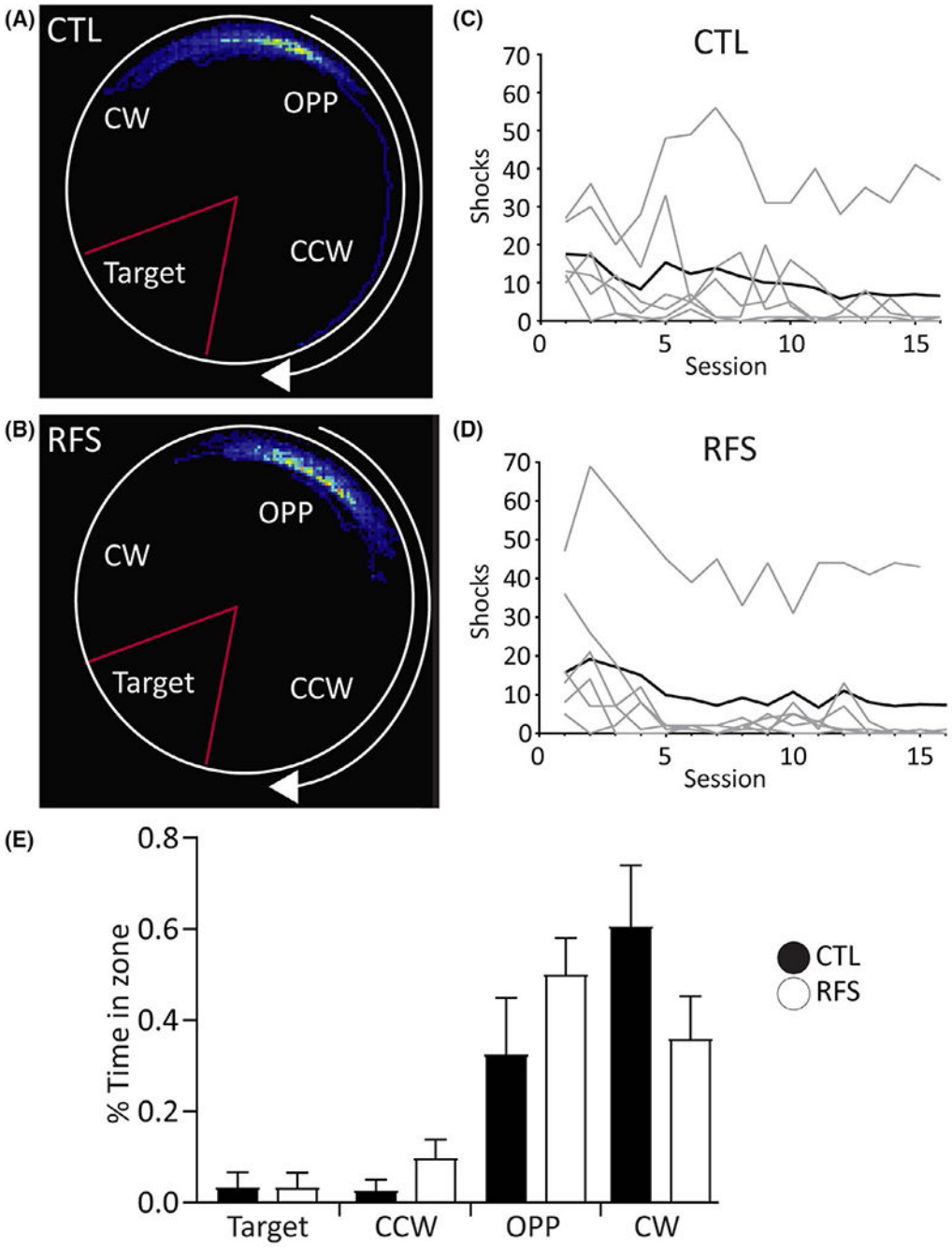

FIGURE 1.

Spatial memory in experimental recurrent febrile seizure (eRFS) rats is unaffected compared with control (CTL). (A, B) Dwell time heat map of Session 16 showing a representative CTL (A) and eRFS (B) rat during the active avoidance task. Shock zone (Target) is denoted by a red triangle. CCW = counterclockwise; CW = clockwise, OPP = opposite. (C, D) Shocks per session (1–16) for CTL (C; $n = 6$) and eRFS (D; $n = 6$) rats. Gray lines = individual rats; black lines = averaged shocks for entire group. Each group contains five rats that met task criterion. (E) Mean percent time in zone for each group for Session 16. The

majority of time spent in CW and OPP zone denotes the use of a spatial avoidance strategy in both groups. Filled bars = CTL; empty bars = eRFS. Data are presented as mean ± SE

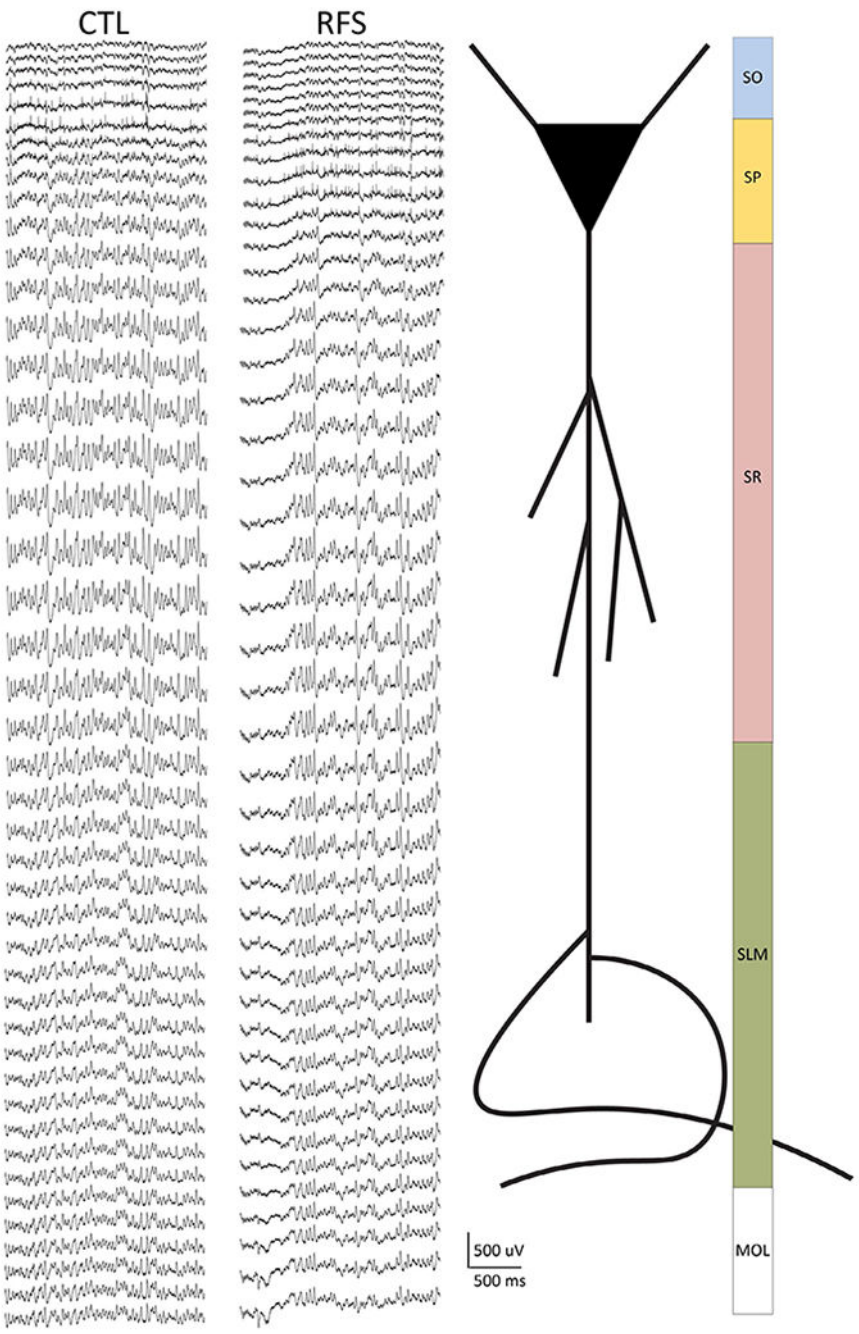

FIGURE 2.

Recordings were made along the somatodendritic axis of CA1 using 64-channel laminar silicon probes in control (CTL) and experimental recurrent febrile seizure (eRFS) rats. Left: Example traces (2 s) from CTL and eRFS recordings showing the resolution of 20-μm spacing (1280 μm total) from the laminar probe. Spikes are visible on channels 5–7 (CTL) and 8–12 (eRFS) to illustrate close but variable distribution of the probe within the tissue. Stratum pyramidale (SP) was used as a reference point for probe placement during the experiment. Right: schematic of where the depth of the recording corresponds to a cartoon

CA1 neuron and corresponding synaptic input regions along the somatodendritic axis. MOL, molecular layer of dentate gyrus; SLM, stratum lacunosum moleculare; SO, stratum oriens; SR, stratum radiatum

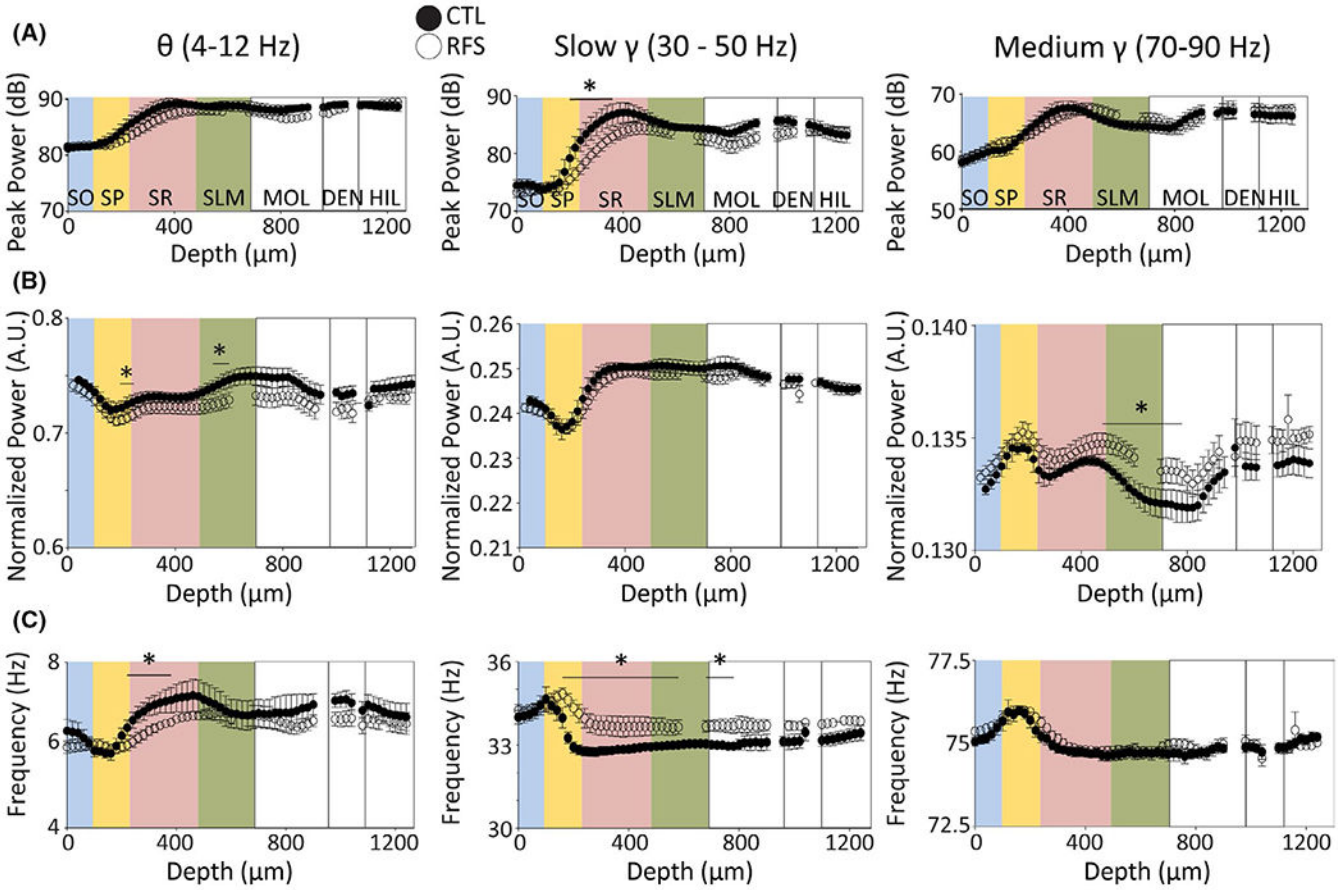

FIGURE 3.

Early life experimental recurrent febrile seizures (eRFSs) alters spectral properties within the theta and gamma bandwidths compared with control (CTL). For all plots, relative CA1 location corresponding to depth is superimposed in colors: blue = stratum oriens (SO), yellow = stratum pyramidale (SP), pink = stratum radiatum (SR), green = stratum lacunosum moleculare (SLM). White = dentate gyrus molecular layer (MOL), dentate gyrus cell layer (DEN), hilus (HIL). For all plots, filled circles = CTL, empty circles = eRFS. (A) Peak power measured in decibels plotted by depth in micrometers for theta (4–12 Hz, left), slow gamma (30–50 Hz, middle), and medium gamma (70–90 Hz, right) bandwidths. (B) Power normalized to the peak shown in arbitrary units (A.U.) plotted against depth for theta (left), slow gamma (middle), and medium gamma (right). (C) Frequency in hertz plotted by depth for theta (left), slow gamma (middle), and medium gamma (right). All statistical analyses were performed using generalized linear models. Statistical significance of $p < .05$ is denoted by asterisk/horizontal bar over the relevant depth measurements; only significant channel-by-channel group × depth interactions are noted. CTL, $n = 5$; eRFS, $n = 6$. eRFSs led to significant changes in expression of theta frequency, slow gamma power and frequency, and normalized medium gamma power throughout CA1 compared with CTL

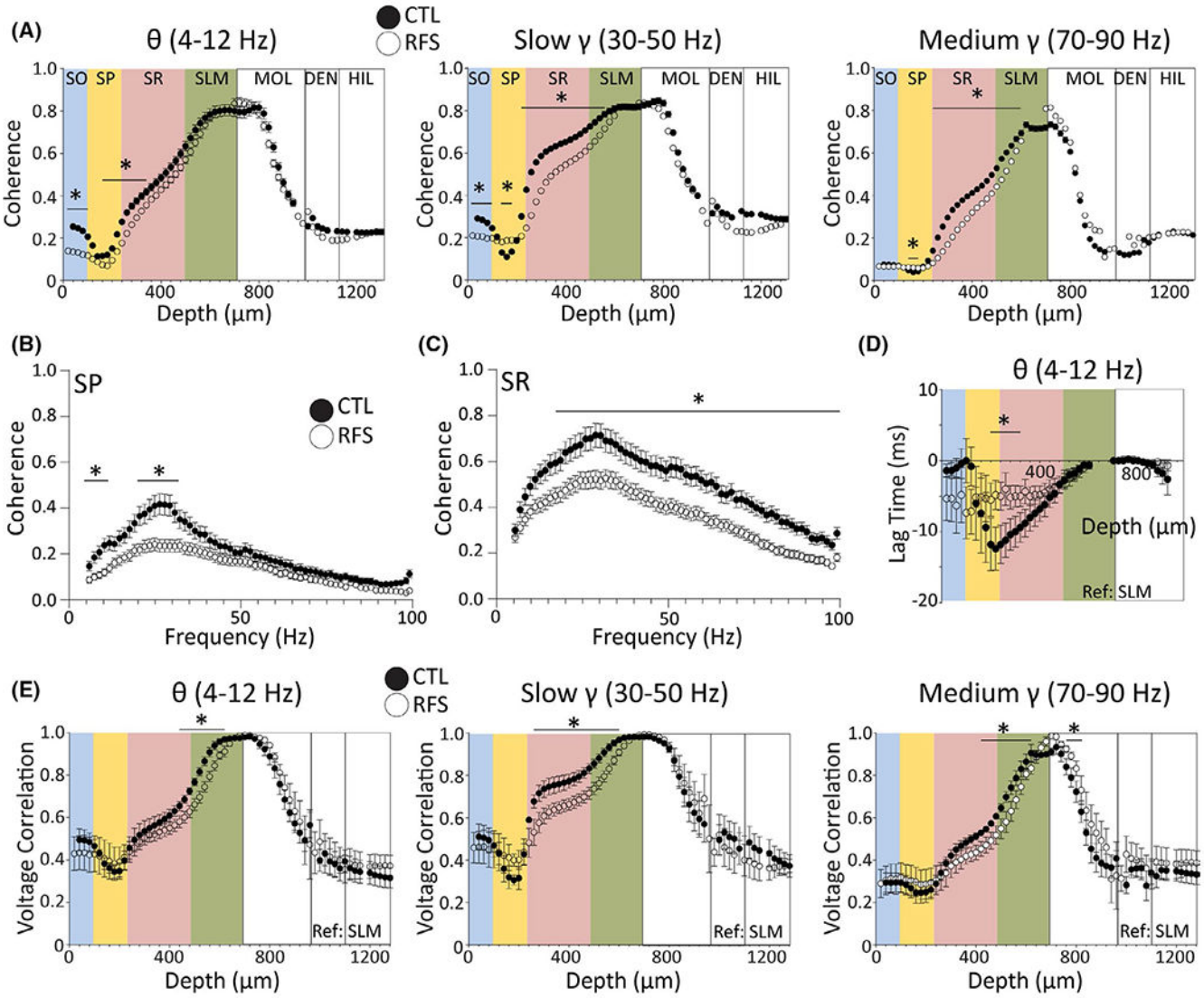

FIGURE 4.

Experimental recurrent febrile seizures (eRFSs) decrease the efficacy of signal propagation along the somatodendritic axis. (A) Phase coherence (referenced to stratum lacunosum moleculare [SLM]) for control (CTL) and eRFS rats plotted as a function of depth (μm) for theta (4–12 Hz, left), slow gamma (30–50 Hz, middle), and medium gamma (70–90 Hz, right) bandwidths. Filled circles = CTL; empty circles = eRFS. Phase coherence exhibits a distinctive pattern along the CA1 somatodendritic axis. The coherence peak was at the reference region and the trough was at stratum pyramidale (SP) for both groups across all bandwidths. (B, C) Phase coherence plotted by frequency (step size = ~1 Hz) for SP (B; probe depth = 100–180 μm) and stratum radiatum (SR; C; probe depth = 280–400 μm) referenced to SLM. Filled circles = CTL; white circles = eRFS. (D) Voltage correlation analysis of lag time, indicating when the reference local field potential (LFP) channel (SLM) was leading or following the target LFP channel (all other depths) for the theta bandwidth. Theta exhibits a dynamic time lag by depth that is corrected at SP, whereas

eRFS remains largely stable throughout. (E) Voltage correlation measurements plotted by depth for theta (left), slow gamma (middle), and medium gamma (right). Filled circles = CTL; empty circles = eRFS. For all plots, relative CA1 location corresponding to depth is superimposed in colors: blue = stratum oriens (SO), yellow = SP, pink = SR, green = SLM. White = dentate gyrus molecular layer (MOL), dentate gyrus cell layer (DEN), hilus (HIL). Filled circles = CTL, empty circles = eRFS. All statistical analyses were performed using generalized linear models. CTL, $n = 5$; eRFS, $n = 6$. In CA1, inputs propagate more effectively along the somatodendritic axis than eRFSs as measured by coherence and voltage correlation. $*p < .05$

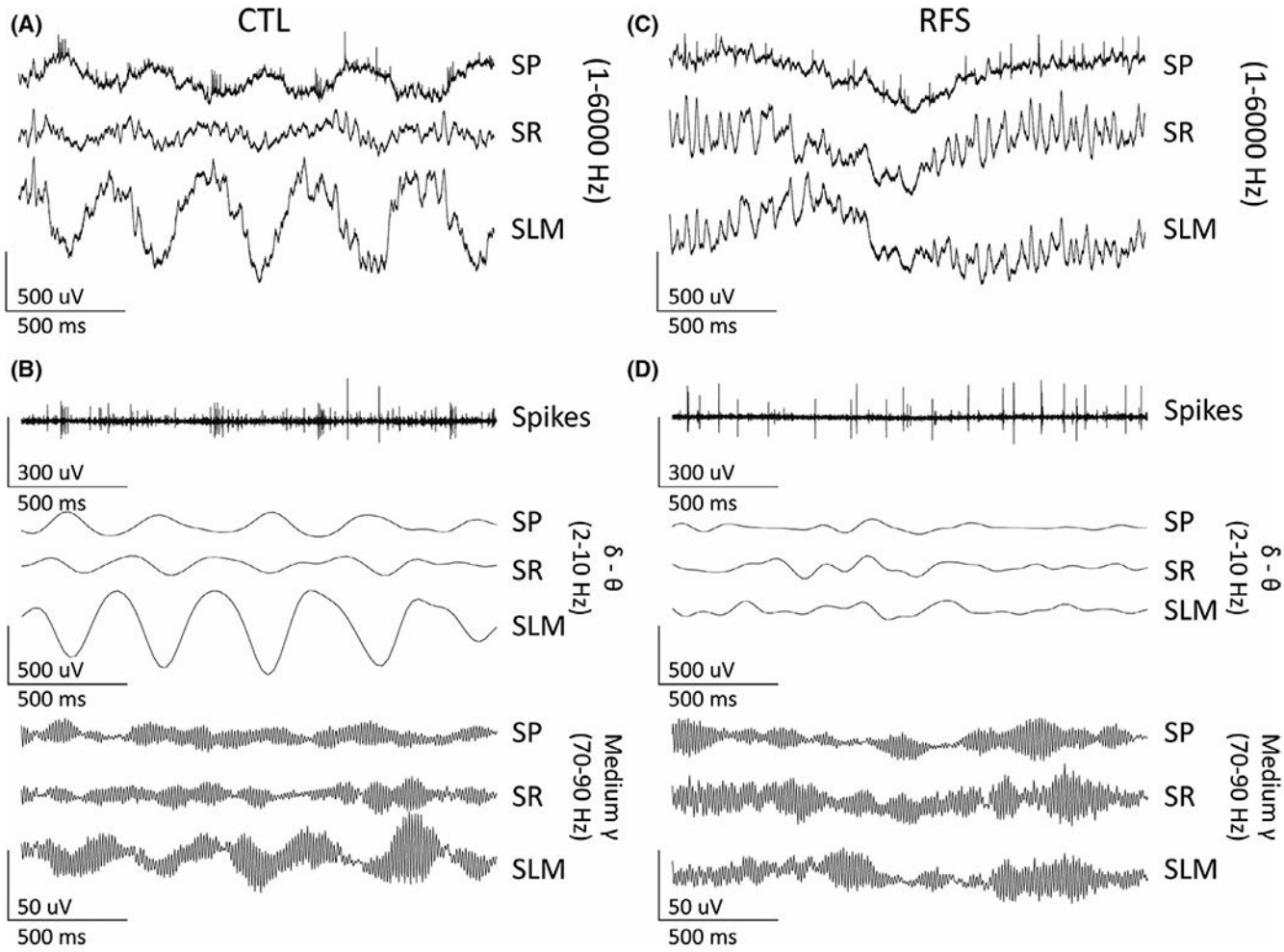

FIGURE 5.

Representative spontaneous local field potentials (LFPs) recorded from control (CTL) and experimental recurrent febrile seizure (eRFS) CA1 to demonstrate bandwidths used in the phase preference analysis. All traces represent 2 s of LFPs. (A) Wideband (1–6000 Hz) LFPs from CTL for stratum pyramidale (SP; top), stratum radiatum (SR; center), and stratum lacunosum moleculare (SLM; bottom). (B) The same trace as A filtered to show representative single units (300–6000 Hz) in SP (top); delta–theta oscillations (2–10 Hz) in SP, SR, and SLM (center three traces); and medium gamma (70–90 Hz) oscillations for SP, SR, and SLM (lower three traces). (C, D) The same for eRFS

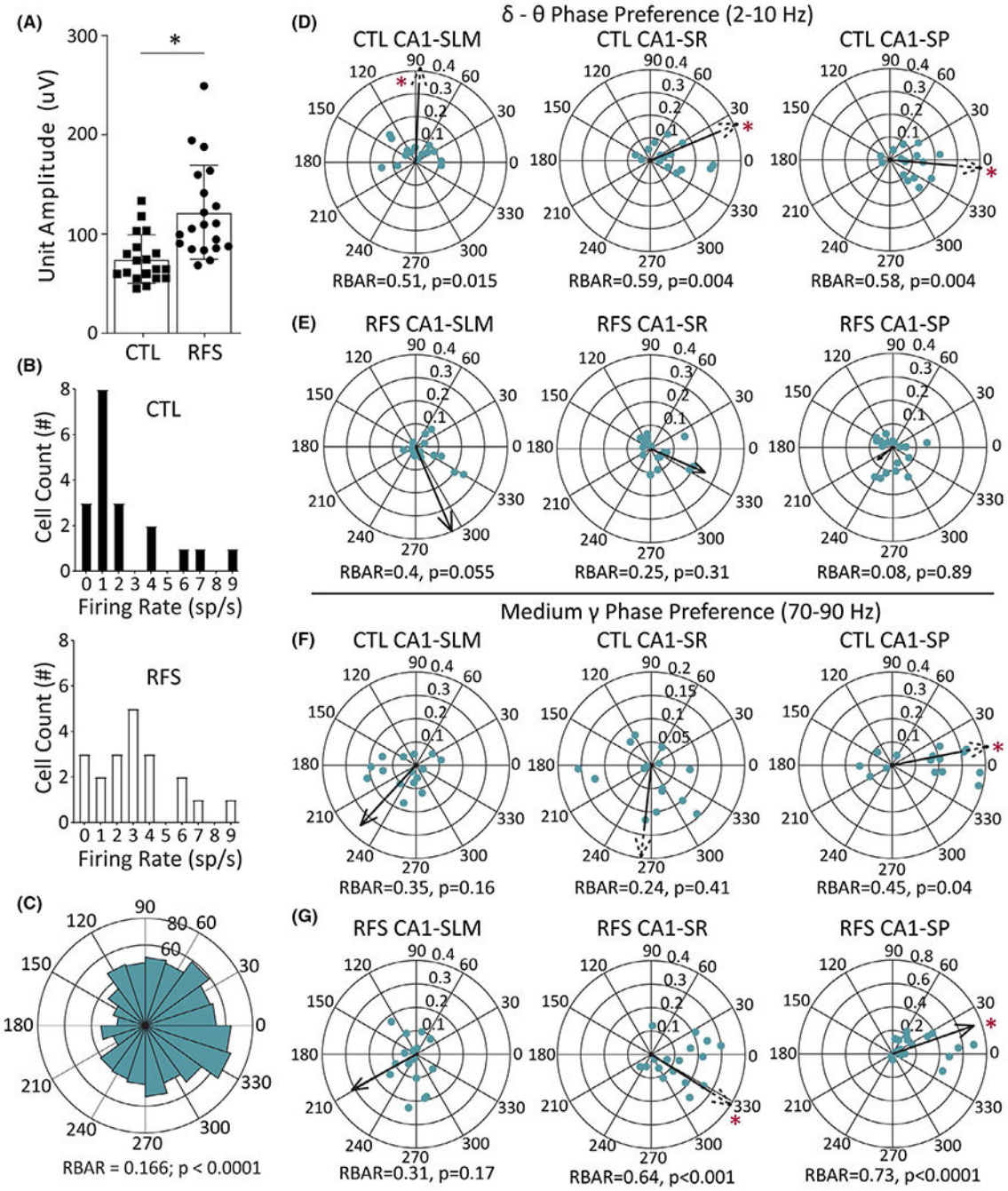

FIGURE 6.

Experimental recurrent febrile seizure (eRFS) CA1 action potentials recorded from single neurons in stratum pyramidale (SP) demonstrate altered firing properties and phase preference when compared to control (CTL). (A) Mean unit amplitude of CTL and eRFS single units in microvolts as measured by the automated cluster-cutting MATLAB package Kilosort. Filled shapes represent mean amplitude from individual units measured (CTL, n = 18; eRFS, n = 20), showing a significantly different size determined by Mann–Whitney test. (B) Distribution of firing rate (spikes [sp]/s) for unit clusters in CTL (top, filled bars)

and eRFS (bottom, empty bars), showing a significantly different distribution of firing rates between groups using Kolmogorov–Smirnov test (CTL, $n = 18$; eRFS, $n = 20$). (C) Representative example of a rose plot used to calculate phase preference for each cell. (D) Phase preference calculated for CTL neuron population against delta–theta (2–10 Hz) oscillations in stratum lacunosum moleculare (SLM; left), stratum radiatum (SR; middle), and SP (right) showing how phase preference changes as the local field potentials ascend the somatodendritic axis (CTL, $n = 18$; eRFS, $n = 15$). Each dot represents a cluster/neuron. Population phase angle and RBAR are denoted by the direction and relative length of the arrow. A dashed arrow was used to represent RBAR when it extended beyond the plot for visualization purposes. Phase angle is shown surrounding each circular plot. RBAR and p-values are given below each circular plot. (E) Phase preference of eRFS neuron populations to delta–theta oscillation for SLM (left), SR (middle), and SP (right; CTL, $n = 18$; eRFS, $n = 15$). (F, G) Corresponding phase preference for CTL (F) and eRFS (G) neuronal populations to the medium gamma (70–90 Hz) oscillation in SLM (left), SR (middle), and SP (right). Statistical significance of $p < .05$ is denoted by asterisk as determined by Mann–Whitney test (A), Kolmogorov–Smirnov test (B), and Rayleigh test for nonuniformity (D–G). CTL cells are slower and smaller on average and are tuned to slow frequencies, whereas eRFS cells are more sensitive to gamma oscillations